Kinetics of Methylmercury Production Revisited

Todd A. Olsen[†], Katherine A. Muller, Scott L. Painter, Scott C. Brooks[*]

AUTHOR ADDRESS: Environmental Sciences Division, Oak Ridge National Laboratory, P.O. Box 2008, MS 6038, Oak Ridge, TN, 37831-6038

AUTHOR INFORMATION

***Corresponding Author:** Scott Brooks, Environmental Sciences Division, Oak Ridge National Laboratory, P.O. BOX 2008 MS 6038, Oak Ridge, Tennessee 37831-6038; e-mail: brookssc@ornl.gov; telephone: 865-574-6398; Fax: 865-576-8646.

†**Present Address:** Geosnytec Consultants, 3043 Goal Canal Drive, Suite 100, Rancho Cordova, CA, 95670.

KEYWORDS: mercury, methylmercury, methylation, demethylation, availability, kinetics

TOC art

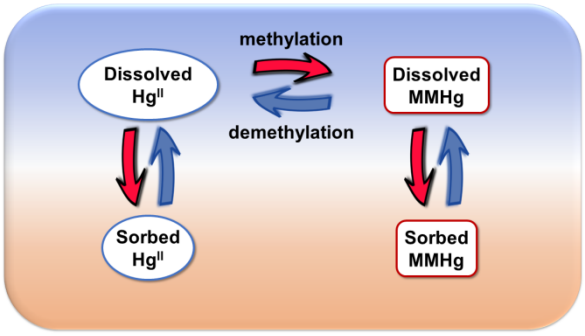
methylation
Dissolved Hg^{II}
Dissolved MMHg
demethylation
Sorbed Hg^{II}
Sorbed MMHg

ABSTRACT.

Laboratory measurements of the biologically mediated methylation of mercury (Hg) to the neurotoxin monomethylmercury (MMHg) often exhibit kinetics that are inconsistent with first-order kinetic models. Using time-resolved measurements of filter passing Hg and MMHg during methylation/demethylation assays, a multisite kinetic sorption model, and re-analyses of previous assays, we show that competing kinetic sorption reactions can lead to time-varying availability and apparent non-first-order kinetics in Hg methylation and MMHg demethylation. The new model employing a multi-site kinetic sorption model for Hg and MMHg can describe the range of behaviors for time-resolved methylation/demethylation data reported in the literature including those that exhibit non first-order kinetics. Additionally, we show that neglecting competing sorption processes can confound analyses of methylation/demethylation assays, resulting in rate constant estimates that are systematically biased low. Simulations of MMHg production and transport in a hypothetical periphyton biofilm bed illustrate the implications of our new model and demonstrate that methylmercury production may be significantly different than projected by single-rate first-order models.

INTRODUCTION

Mercury (Hg) is a toxic element that occurs naturally and as an anthropogenic pollutant in the environment. The neurotoxin monomethylmercury (MMHg) is of particular concern since it has adverse developmental effects on young children and developing embryos at low levels and biomagnifies in aquatic environments. MMHg is rarely a direct pollutant, but is formed in the environment from Hg^{II} in a microbially mediated process called Hg methylation. Since MMHg is the main vector for human exposure to Hg there has been significant effort to measure Hg methylation and MMHg demethylation rates, along with controls on these rates, in various environmental settings [1-19].

Early studies added radioactive tracers ($^{203}HgCl_2$ and $^{14}CH_4HgCl$) to environmental samples and monitored their transformation in an attempt to determine methylation and demethylation rates [12, 20]. A limitation of this approach is the need to add Hg species well above ambient sample concentrations,

particularly for MMHg, because of high detection limits. In response, methods were developed using stable Hg isotopes where spiking at sub-ambient tracer levels is possible [8]. However, there is still a question of the impact the speciation state and bioavailability of the added tracers (usually as $HgCl_2$ and MMHgCl) have on the resulting methylation and demethylation rate constants and whether these rate constants extrapolate to ambient systems where the Hg is in a different and dynamic speciation state. Additionally, the bioavailability of the tracers likely changes during the course of the experiment as they are exposed to the various ligands and sorption sites in the sample matrix [13]. Monitoring these dynamics and incorporating them into a model may be crucial when applying these techniques to determine methylation and demethylation rate constants. In this paper, we use the term 'available' to refer to that fraction of the total Hg or MMHg in a system that passes a 0.2 μm pore size filter. We define methylation and demethylation rates relative to the pool of filter-passing Hg and MMHg. However, the chemical speciation of mercury in the dissolved phase also influences bacterial uptake and methylation of mercury[21, 22], and as a result, some of the filter-passing Hg or MMHg may also be unavailable.

Most scientists have adopted a first-order reversible kinetic model to describe their Hg methylation and MMHg demethylation assays [9]:

$$\frac{d[MMHg]}{dt} = k_m[Hg^{II}] - k_d[MMHg] \qquad (1)$$

$$\frac{d[Hg^{II}]}{dt} = -k_m[Hg^{II}] + k_d[MMHg] \qquad (2)$$

where k_m = methylation rate constant (d^{-1}); k_d = demethylation rate constant (d^{-1}); $[Hg^{II}]$ = concentration of inorganic Hg; and [MMHg] = concentration of MMHg. Commonly, equations (1) and (2) are simplified so that single time point data can be used to determine k_m and k_d [2, 3, 6, 7, 16-18]. As we showed in a previous paper [18], when using this approach, the results can depend on the length of the experiment and the initial tracer concentrations. This highlights the importance of using time series data when

78 determining k_m and k_d. Studies that report time series data often show non-first-order behavior which
79 results in a poor model fit using equations (1) and (2) [2, 4, 6, 8, 9, 11, 13, 14, 18, 19, 23].

80 Apparent non-first-order dynamics in MMHg tracer concentration does not necessarily imply
81 non-first-order kinetics in methylation and demethylation. Instead, there may be competing kinetic
82 reactions that convert Hg^{II} and MMHg to states that are not bioavailable during the assay. Many methods
83 have been proposed to measure bioavailable Hg including filter passing species; diffusive gradient thin-
84 film samplers [24]; chemical selective extraction [25]; direct ethylation [26]; and stannous chloride reduction
85 (SnRHg)[16, 26]. Alternatively, speciation calculations have been used to estimate the bioavailable fraction
86 of the Hg^{II} or MMHg based on ancillary measurements [27]. Although a consensus method has not
87 emerged, these methods all suggest that only a small fraction of the total Hg^{II} or MMHg are available for
88 methylation or demethylation, respectively, in natural systems.

89 Few studies have used bioavailable ambient Hg^{II} measurements instead of total Hg^{II} in equation
90 (1) and (2) in their estimates of net Hg methylation in different environmental compartments [10, 15, 16].
91 However, only one study accounted for changing tracer bioavailability during the course of a Hg^{II}
92 methylation assay [13]. Specifically, Lehnherr et al. (2011)[13] proposed an analytical solution to equation (1)
93 that included reversible loss of the available Hg^{II} tracer during bioassay incubations. We could find no
94 studies that included changing MMHg tracer bioavailability in their model.

95 The motivation for studying methylation/demethylation in the laboratory is to build models to
96 predict MMHg levels in natural systems over time. Clearly, time-varying bioavailability has the potential
97 to affect both the model structure and inferred values of the rate constants k_m and k_d, and is thus critically
98 important to understand and quantify. Here we quantify kinetics of methylation/demethylation tracers
99 using a new model, experiments, and re-analysis of previous experiments. We propose a new multisite
100 kinetic sorption model to represent transfers of Hg^{II} and MMHg tracers between dissolved and sorbed
101 states during a bioassay and compare that model to time-resolved measurements of Hg^{II} and MMHg
102 concentrations. We then combine the sorption model with the first-order methylation/demethylation
103 model and re-analyze methylation/demethylation assays on periphyton biofilm from a Hg contaminated

watershed [18] to produce new estimates of k_m and k_d. Finally, the implications of this new approach are examined in model simulations of MMHg production and transport in periphyton on a stream bed.

MATERIALS AND METHODS

Model for transient Hg and MMHg tracer availability

Assuming first order kinetics for reversible Hg sorption on fast and slow sites and reversible conversion between Hg^{II} and Hg^0, mass conservation is expressed as:

$$\frac{d[Hg]}{dt} = -k_1[Hg] + k_2[Hg_f] - k_3[Hg] + k_4[Hg_s] - k_5[Hg] + k_6[Hg^0] \quad (3)$$

$$\frac{d[Hg_f]}{dt} = k_1[Hg] - k_2[Hg_f] \quad (4)$$

$$\frac{d[Hg_s]}{dt} = k_3[Hg] - k_4[Hg_s] \quad (5)$$

$$\frac{d[Hg^0]}{dt} = k_5[Hg] - k_6[Hg^0] \quad (6)$$

where k_1 = Hg^{II} fast site adsorption rate constant; k_2 = Hg^{II} fast site desorption rate constant; k_3 = Hg^{II} slow site adsorption rate constant; k_4 = Hg^{II} slow site desorption rate constant; k_5 is the rate constant for conversion of Hg^{II} to Hg^0; k_6 is the rate constant for conversion of Hg^0 to Hg^{II}; Hg_f = amount of Hg^{II} sorbed to the fast sites; Hg_s = amount of Hg^{II} sorbed to the slow sites;

The corresponding equations describing changing MMHg availability are:

$$\frac{d[MMHg]}{dt} = -k_7[MMHg] + k_8[MMHg_f] - k_9[MMHg] + k_{10}[MMHg_s] \quad (7)$$

$$\frac{d[MMHg_f]}{dt} = k_7[MMHg] - k_8[MMHg_f] \quad (8)$$

$$\frac{d[MMHg_s]}{dt} = k_9[MMHg] - k_{10}[MMHg_s] \quad (9)$$

where k_7 = MMHg fast site adsorption rate constant; k_8 = MMHg fast site desorption rate constant; k_9 = MMHg slow site adsorption rate constant; k_{10} = MMHg slow site desorption rate constant; $MMHg_f$ = amount of MMHg sorbed to the fast sites; and $MMHg_s$ = amount of MMHg sorbed to the slow sites. Rate constants for equations (3)-(9) were determined from experiments independent of the methylation/demethylation assays (see below).

Methylation/demethylation model with changing tracer availability

The equations describing the changing availability can be merged with the methylation/demethylation model (equations (1) and (2)) when using either a methylation tracer or demethylation tracer. Adding a methylation ($k_m[Hg]$) and demethylation ($k_d[MMHg]$) term to equations (3) and (7) results in equations (10) and (11), respectively:

$$\frac{d[Hg]}{dt} = -k_m[Hg] + k_d[MMHG] - k_1[Hg] + k_2[Hg_f] - k_3[Hg] + k_4[Hg_s] - k_5[Hg] + k_6[Hg^0] \quad (10)$$

$$\frac{d[MMHg]}{dt} = k_m[Hg] - k_d[MMHg] - k_7[MMHg] + k_8[MMHg_f] - k_9[MMHg] + k_{10}[MMHg_s] \quad (11)$$

Equations (4)-(6) and (8)-(11) represent the complete model that accounts for changing Hg^{II} and MMHg tracer availability along with simultaneous methylation and demethylation to both tracer sets during the bioassay. The modeling approach assumes that k_m and k_d are constant over the course of the incubations which may not be valid in all settings such as long incubation times or in field settings.

Modeling approach

Based on the system of first order differential equations, changing availability of Hg^{II} (equations (3)-(6)) and MMHg (equations (7)-(9)) were individually modeled using the ordinary differential equation solver (ode45) in MATLAB R2016a (The MathWorks, Natick, Massachusetts). Model coefficients were estimated using a non-linear fitting routine, nlinfit. The Hg^{II} model was fit to three directly measured data

sets: filter passing Hg (Hg_D), total sorbed Hg^{II}, and dissolved Hg^0, weighted by the standard deviation of each data set. The MMHg model was fit to the directly measured filter passing MMHg ($MMHg_D$). The overall methylation/demethylation model was fit to the $MM^{201}Hg$ and $MM^{202}Hg$ data sets, weighted by the standard deviation, by adjusting the value of k_m and k_d while holding k_1-k_{10} constant at the values previously estimated. 95% confidence bands around the model fits to the data were determined by conducting a Monte Carlo analysis (n=10,000) where $k_{1\text{-}10}$ and k_m and k_d were sampled randomly from a multivariate normal distribution based on the fitted parameters and their corresponding covariance matrices.

A global sensitivity analysis of the model was conducted using MMHg concentration at three days as the model metric with Sobol sampling of the parameter space. The global sensitivity analysis toolbox in MATLAB, GSAT developed by Cannavó (2012)[28] was used to determine the sensitivity indices (Fig. S3 and S4).

Filter passing Hg^{II} (Hg_D) and filter passing MMHg ($MMHg_D$) methods

We chose filter passing Hg^{II} (Hg_D) and filter passing MMHg ($MMHg_D$) as our proxy measurements for available Hg^{II} and MMHg. These experiments were designed to monitor the change in partitioning of the added Hg^{II} and MMHg tracers during periphyton bioassays which could then be applied to our previously published methylation/demethylation time series data set to determine k_m and k_d[18]. Fresh wet periphyton samples were weighed out equivalent to 0.1 g-dry weight either in 60 mL glass I-Chem jars for the Hg_D experiment or 40 mL VOA vials for the $MMHg_D$ experiment. To each vessel 25 mL 18.2 MΩ × cm water and 1000 ng $^{201}Hg^{II}$ or 1 ng $MM^{202}Hg$ (similar to the Hg^{II} and MMHg tracer masses added during bioassays) were added[18]. Samples were sacrificed over time and Hg_D or $MMHg_D$ were measured. In the Hg^{II} experiment triplicate samples were taken at 1, 5, and 20 minutes and 1, 2, 4, 8, 14 and 22 hours. In the MMHg experiment triplicate samples were taken at 1 and 25 minutes and 1, 2, 3, 6, 8, 12, 22 and 28 hours.

In the Hg^{II} experiments the Hg_D, total sorbed Hg, and dissolved Hg^0 were directly measured. To measure dissolved Hg^0 100 µL of the 25 mL sample was subsampled into a purging vessel and the Hg^0 was purged onto a gold trap. The gold trap was then heated while the carrier gas was fed into an ELAN DRC-e ICP-MS for detection. To measure Hg_D the 25 mL samples were filtered through a 0.2 µm polyethersulfone (PES) filter, acidified to 0.5% HCl, then analyzed following United States Environmental Protection Agency (USEPA) Method 1631 using ICP-MS detection[29]. To measure the total sorbed Hg the filters were digested in 12 mL aqua regia. The filters were digested in the same jar as the experiment so Hg sorbed to container walls would be combined with the filter retained Hg resulting in the total sorbed Hg. The extract was then diluted and analyzed following USEPA 1631 using ICP-MS detection [29]. Since the amount of MMHg formed from the Hg^{II} tracer was only 0.1% it was ignored as a sink for the Hg^{II}. Hg_D and Hg^0 samples were analyzed within 24 hours of collection. Total sorbed Hg was analyzed within four days of sample collection.

In the MMHg sorption experiments there was the potential that the MMHg tracer could be demethylated on a large enough scale to impact the results. Killed controls were run where the samples were autoclaved or frozen then thawed prior to tracer addition. Additionally, samples were refrigerated (4 °C) prior to tracer addition and then for the duration of the experiment. The killed control samples showed significantly larger $MMHg_D$ than the refrigerated samples and in a parallel experiment no demethylation was found in the refrigerated samples. We believe the methods used to kill the sample also changed their sorption and ligand properties which resulted in larger $MMHg_D$ in those experiments. An additional short term experiment compared MMHg sorption onto untreated periphyton held at room temperature, autoclaved periphyton, and periphyton refrigerated at 4°C (Fig. S6). MMHg sorption onto refrigerated periphyton was comparable to the untreated periphyton. MMHg sorption onto autoclaved periphyton was substantially lower. Preliminary experiments showed there was a small but statistically significant ($p = 0.012$) demethylation in addition to MMHg sorption for untreated samples kept at room temperature. There was no measurable demethylation in the refrigerated samples (Fig. S7). Therefore, we chose the refrigeration treatment when conducting the final $MMHg_D$ experiments. To measure

$MMHg_D$ the 25 mL samples were filtered through a 0.2 μm PES filter, acidified to 0.5% HCl, and analyzed the next day following USEPA Method 1630 using ICP-MS detection [30]. We tested for and could not detect the MMHg tracer as Hg^0 during the $MMHg_D$ experiments.

RESULTS AND DISCUSSION

Quantifying Hg and MMHg availability

The time series methylation/demethylation data set from Olsen et al. 2016 [18] exhibited non-first order behavior resulting in poor model fit using equations (1) and (2). They hypothesized that MMHg might have formed during extraction and included an intercept value in the methylation model to account for that potential artifact. Subsequent experiments revealed no MMHg artifact formation (data not shown). With that new information, it is apparent that the Olsen et al. 2016 time series data exhibits an initially fast rate of MMHg formation followed by a slower formation rate at later times. This observation and similar results from others [2, 8, 9, 11, 13, 18, 19, 23] led us to investigate the role of competition from sorption processes during the experiment as the explanation for the multiple time-scale behavior.

We performed experiments similar to Olsen et al. (2016)[18] and monitored the change in partitioning of the introduced Hg^{II} and MMHg tracers. Although there is no consensus method for the direct measurement of available Hg and MMHg, sorption reactions are expected to dominate the changing Hg and MMHg availability when a solid matrix such as periphyton is present. For that reason, we chose 0.2 μm filter passing Hg (Hg_D) and MMHg ($MMHg_D$) as proxy measurements for available Hg and MMHg. Additionally, we measured SnRHg for the Hg^{II} tracer and found similar behavior to Hg_D (Fig. S5).

The goals of the Hg^{II} and MMHg sorption experiments were to evaluate sorption kinetics independently from Hg methylation and MMHg demethylation and to inform kinetic models that account for competition between sorption and methylation. We consider a conceptual model (Fig. 1) in which available forms of Hg and MMHg coexist with unavailable forms resulting from sorption onto sites in the sample. The Hg and MMHg added as $HgCl_2$ and MMHgCl, respectively, are presumably fully available

217 initially, but as Hg and MMHg associate with the ligands and sorption sites in the sample some fraction
218 becomes unavailable for methylation/demethylation. Because kinetics with at least two time scales are
219 frequently reported in the metal sorption literature [31-34], we chose to describe Hg^{II} (equations (3)-(6)) and
220 MMHg (equations (7)-(9)) availability changes using first-order reversible sorption on two types of sites
221 (fast and slow) characterized by two pairs of rates (forward and reverse)[34]. We unsuccessfully attempted
222 to fit the sorption data with alternative models including one that explicitly included a finite sorption
223 capacity[35]. Moreover, the additional complexity in that model does not appear necessary to fit the
224 available data. We note that the rate constant could be written as a product of specific surface area, areal
225 site densities, and an intrinsic rate defined on a per site basis. Without explicit limitations on the available
226 sites and neglecting competition from other metal cations, our representation in terms of an effective rate
227 constant is equivalent. Competition from other metal cations could be of interest in some applications,
228 but is not relevant for the conditions of our experiments. Additionally, reversible reduction of Hg^{II} to Hg^0
229 is included. Governing equations are provided in the methods section.
230 Results of the Hg^{II} and MMHg sorption experiments (Figs. 2 and 3 and Figs. S1 and S2)
231 exhibited kinetics with at least two scales, consistent with previous results in the metal sorption literature
232 [31, 33, 34]. Specifically, within one minute of the Hg^{II} addition, the Hg_D dropped to 40% of the total mass
233 added and then continued a slower decline over the next 22 hours with the final measurement at 1% of the
234 total mass added. The Hg^0 concentration slowly increased and then decreased, but never exceeded 7% of
235 the total mass of Hg^{II} added. $MMHg_D$ exhibited similar behavior to Hg_D. After one minute, the $MMHg_D$
236 had decreased to 60% of its initial value and continued to drop to 10% after 24 hours. Negative controls
237 and extensive testing of filters and labware ruled out sorption onto these materials as the cause of the
238 rapid and extensive loss of Hg and MMHg from solution. Additionally, ancillary control experiments
239 described in Olsen (2016) verified there was no photodemethylation or photoreduction in our
240 experiments.
241 Figs. 2 and 3 show the best-fit model results and the corresponding 95% confidence bands using
242 our two-site reversible sorption model. Although there are some minor mismatches between the model

and experiment in the Hg^{II} concentration around 3.5×10^{-3} days and at 1 day, the sorbed and dissolved concentration of Hg^{II} and the dissolved concentrations of MMHg and Hg^0 are reasonably well represented over the entire experiment. Best-fit values of the rate constants are provided in Tables S1 and S2. Other researchers wishing to apply this model should determine $k_1 - k_{10}$ for their experimental systems until such time that consensus representative values are available for different settings (e.g., freshwater versus marine systems, contaminated versus uncontaminated systems).

This model framework can easily be adapted for single site (one scale kinetic) behavior, as seen in the SnRHg data from Lehnherr et al. (2011)[13], by omitting equations (5) and (6) and the corresponding terms in equation (3). Similarly, additional or irreversible terms can be included. Alternative kinetic expressions of Hg isotope availability during lab experiments can be readily incorporated into this model. The gas/liquid partitioning of Hg^0 can be included in this model, but was not included here because mass balance was achieved with the measurements of Hg_D, total sorbed Hg and dissolved Hg^0. In a well-mixed sample with high Hg^0 formation, the gas/liquid partitioning may be an important component to the loss of bioavailable Hg.

Model application to Olsen et al. 2016 time-series data

The new model, incorporating changing tracer availability, was applied to the only methylation/demethylation time course data set from Olsen et al. (2016) to determine k_m and k_d (Fig. 4)[18]. Those experiments were conducted with periphyton biofilms grown in the creek (comprising a complex assemblage of biotic, detrital, and inorganic components in an exopolymeric matrix) and unfiltered ambient creek water collected immediately before use. The resulting model fit was able to reproduce the initial surge in the methylation tracer ($MM^{201}Hg$) observed in the methylation data set (Fig. 4). The methylation rate constant is significantly larger in the new model ($35 \pm 4 \times 10^{-5}$ d^{-1}) when compared to the value reported in Olsen et al. (2016) ($1.42 \pm 0.32 \times 10^{-5}$ d^{-1}). This was expected since the new model needed to compensate for the loss of available Hg^{II} during the bioassay. The k_d value showed a smaller relative increase than the k_m estimate in the new model ($9.2 \pm 2.4 \times 10^{-2}$ d^{-1}) than the previous model (1.77

269 $\pm 0.63 \times 10^{-2}$ d^{-1}). Our finding that methylation and demethylation tracer kinetics is consistent with
270 changing availability during bioassays suggests that previous studies using initially dissolved Hg tracers
271 that did not account for these processes may have systematically underestimated k_m and k_d. Studies that
272 introduce Hg as sorbed or precipitated phases [11, 36, 37] result in lower inferred methylation rate constants
273 compared with studies that introduce dissolved Hg tracer. Rate constants inferred by monitoring total
274 mercury (solid and dissolved) are effective values that include the effects of rate-limited desorption and
275 dissolution and do not directly provide information on the rate constants for methylation of dissolved
276 mercury unless the desorption or dissolution kinetics are also modeled.
277
278 *Model sensitivity analysis*
279 A global sensitivity analysis of the model, using MMHg concentration at three days as the model
280 metric, revealed high sensitivity to the Hg^{II} slow adsorption rate constant (k_3) which constituted 63% of
281 the model variance. The methylation rate constant (k_m; 22%) and the Hg^{II} slow desorption rate constant
282 (k_4, 13%) were also sensitive determinants of model output (Fig. S3 and S4). The remaining parameters
283 combined to account for less than 2% of model variance.
284 Methylation and demethylation data sets reported in the literature exhibit a range of behaviors,
285 many of which do not follow first-order kinetics [2, 4, 6, 8, 9, 11, 13, 14, 18, 19]. In the literature there are two types
286 of behavior exhibited in methylation tracer data sets: 1) Initially fast followed by a slower increase in the
287 MMHg methylation tracer [2, 4, 8, 9, 11, 13, 18, 19], and 2) Increase followed by a decrease of the MMHg
288 methylation tracer [6, 8, 11, 13, 14, 23]. Similarly there are two types of demethylation behavior exhibited: 1)
289 gradual decrease in the MMHg demethylation tracer [13, 14, 18], and 2) fast decrease followed by a slower
290 decrease in the MMHg demethylation tracer [6, 9, 14].
291 Forward model simulations were used to examine the range of behaviors of the new model (first-
292 order methylation and demethylation kinetics while accounting for dynamic tracer availability) while
293 setting the parameters within realistic bounds. Rate constants $k_{1\text{-}10}$ were prescribed (Tables S1 and S2).
294 k_m was set at 0.001 d^{-1} and k_d was varied with values of 1, 10 and 100 d^{-1}. The new model can mimic the

295 different behaviors for methylation and demethylation tracer data sets seen in the literature listed
296 previously (Fig. 5). In other words, our model predicated on first-order methylation and demethylation
297 kinetics exhibited non-first-order behavior because of competing kinetic reactions.
298
299
300 *Implications*
301 To explore implications of neglecting transient availability of Hg and MMHg, we incorporated
302 our model for kinetics of Hg and MMHg in available and multiple non-available states into a model for
303 transport in a hypothetical periphyton mass on a stream bed. Transport is conceptualized as occurring in
304 mobile zones in the periphyton mass, with methylation, demethylation, and sorption reactions occurring
305 in stagnant zones between the flowing channels. A Lagrangian travel-time formulation [38], which uses
306 water travel time τ in place of travel distance and flow velocity, was used for 1-D transport in the mobile
307 zones of the periphyton bed. The travel-time formulation is particularly convenient for generic broad-
308 scope parameter sensitivity exploration because it replaces two key parameters (the reach length and the
309 flow velocity) with a single parameter τ.
310 The conservation equations for solutes in the mobile zone written in the travel-time form were
311 coupled to a reaction-diffusion equation for the interchannel stagnant zones. Governing equations and a
312 description of the solution method may be found in Supplemental Material. We implemented the seven-
313 component system of Fig. 1 as well as the conventional two-component system that includes only Hg^{II}
314 and MMHg with first-order kinetic reactions (equations (1) and (2)) and full availability. The rate
315 constants in Tables S1 and S2 were used in the seven-component model; the methylation and
316 demethylation rate constants for the two-component model were found by fitting to equations (1) and (2),
317 as presented in Olsen et al. (2016)[18]. With kinetic rate constants specified by the above analyses, the only
318 remaining parameters are the size Δ of the immobile zones, the effective diffusion coefficient D_{eff} in the
319 immobile periphyton biofilms, and the specific surface area γ of the immobile zones. We consider a

constant input of Hg^{II} into the upstream side of an initially solute-free periphyton bed and allow the system to come to steady state. The quantity of interest is the MMHg fraction (of the total dissolved mercury) versus water travel time.

Simulated MMHg fractions are shown in Fig. 6 for a representative case with $\Delta = 5$ cm, $D_{eff} = 10^{-9}$ m^2/s and $\gamma = 10^3$ m^{-1}. The MMHg fraction from our availability model is significantly greater than that obtained with equations (1) and (2) for all values of τ. For smaller travel times, the differences are large in relative terms, about one order of magnitude for a travel time of 5 hours. At larger travel times the relative difference is smaller, but still significant. We repeated this analysis for different combinations of the parameters, D_{eff}, γ and found similar trends in all cases considered. That is, neglecting changing availability in this data set results in a low bias in the prediction of MMHg, which is the direct result of biases in the inferred methylation and demethylation rate constants when the two-rate, two-component model was used to analyze the short-duration methylation/demethylation experiments.

The motivation for studying methylation/demethylation in the laboratory is to build models to predict the evolution of MMHg production and migration in natural systems. Our results show that competing kinetic processes can lead to time-varying availability and alter the kinetics of methylation and demethylation. If not properly accounted for when analyzing methylation/demethylation assays, the competing kinetic processes create significant biases in estimated methylation/ demethylation rate constants. Although we chose filter-passing Hg^{II} and MMHg as proxies for the available fraction under the assumption that sorption reactions would dominate availability in the presence of a solid matrix, the new model can readily be applied to other measurements of time-varying availability (e.g., SnRHg). Potential mechanisms for the kinetic sorption processes were not elucidated here, but they would presumably represent the combined effects of surface complexation and physical processes such as diffusion that limit the rates of transfer to available sorption sites.

The use of filter passing Hg and MMHg to estimate availability has its own limitations. The 0.2 μm pore size passing Hg and MMHg included NOM complexes, colloidal, and nanoparticulate phases

each of which likely comprise their own available and nonavailable fractions. As our understanding of those fractions and their dynamics deepens and are incorporated into models, the resulting k_m and k_d estimates will likely be different but the biases introduced from neglecting those processes are likely to remain. Indeed, our use of filter-passing concentrations as proxies for the available Hg and MMHg is likely to underestimate the potential model biases that result from neglecting partitioning to unavailable forms. Regardless of the mechanisms involved or measurement of time-varying availability used, our results clearly show that first-order models that do not account for competing processes that reduce availability will produce significant biases in projections of MMHg production and migration. Using time-resolved measurements in methylation/demethylation assays instead of single-point measurements is essential for avoiding those artifacts.

ACKNOWLEDGEMENTS

This work was funded by the U.S. Department of Energy, Office of Science, Biological and Environmental Research, Subsurface Biogeochemical Research (SBR) Program and is a product of the SBR Science Focus Area (SFA) at ORNL. The isotopes used in this research were supplied by the United States Department of Energy Office of Science by the Isotope Program in the Office of Nuclear Physics.

ADDITIONAL INFORMATION

The authors declare no competing financial interests. Supporting Information accompanies this paper. All data generated or analyzed during this study are included in the Supporting Information file. MATLAB files used in this study and the Mathematica files used to generate Fig. 6 are available from the authors upon request.

SUPPORTING INFORMATION

The Supporting Information includes details on the field-scale transport model, five additional figures and five tables. Supporting Figures 1 and 2 show the simulated dynamics of Hg and MMHg

sorption, respectively, and their partitioning between fast and slow sorption sites. Supporting Figure 3 shows the results of the global sensitivity analysis (GSA) for each model parameter and Supporting Figure 4 shows the normalized sensitivity coefficients and correlation coefficients from the GSA. Figure 5 shows the loss of Sn(II) reducible Hg over time. Figure 6 shows MMHg sorption onto untreated, autoclaved and refrigerated periphyton in short term experiments. Figure 7 shows MMHg demethylation results for untreated versus refrigerated samples during sorption experiments. Supporting Tables 1 and 2 provide the estimated parameter value ± 1 standard error for the Hg and MMHg sorption models, respectively. Supporting Table 3 provides the Hg sorption and Hg^0 data to which the sorption model (equations (3) – (6)) was fit and Supporting Table 4 provided the MMHg data to which the sorption model (equations (7) – (9)) was fit. Supporting Table 5 provides the time-course methylation/ demethylation data from Olsen (2016)[18] to which the multi-compartment model (equations (4)-(6) and (8)-(11)) and the two-compartment model (equations (1) and (2)) were fit to determine k_m and k_d under the scenarios of time-dependent availability and 100% availability at all times, respectively.

384 REFERENCES

385 1. Benoit, J. M.; Gilmour, C. C.; Mason, R. P.; Heyes, A., Sulfide controls on mercury speciation
386 and bioavailability to methylating bacteria in sediment pore waters. *Environ. Sci. Technol.* **1999,** *33*, (6),
387 951-957.
388 2. Desrosiers, M.; Planas, D.; Mucci, A., Mercury methylation in the epilithon of boreal shield
389 aquatic ecosystems. *Environ. Sci. Technol.* **2006,** *40*, (5), 1540-1546.
390 3. Drott, A.; Lambertsson, L.; Bjorn, E.; Skyllberg, U., Do potential methylation rates reflect
391 accumulated methyl mercury in contaminated sediments? *Environ. Sci. Technol.* **2008,** *42*, (1), 153-158.
392 4. Eckley, C. S.; Watras, C. J.; Hintelmann, H.; Morrison, K.; Kent, A. D.; Regnell, O., Mercury
393 methylation in the hypolimnetic waters of lakes with and without connection to wetlands in northern
394 Wisconsin. *Can. J. Fish. Aquat. Sci.* **2005,** *62*, (2), 400-411.
395 5. Gilmour, C. C.; Henry, E. A.; Mitchell, R., Sulfate stimulation of mercury methylation in
396 freshwater sediments. *Environ. Sci. Technol.* **1992,** *26*, (11), 2281-2287.
397 6. Hamelin, S.; Amyot, M.; Barkay, T.; Wang, Y. P.; Planas, D., Methanogens: Principal
398 methylators of mercury in lake periphyton. *Environ. Sci. Technol.* **2011,** *45*, (18), 7693-7700.
399 7. Heyes, A.; Mason, R. P.; Kim, E. H.; Sunderland, E., Mercury methylation in estuaries: Insights
400 from using measuring rates using stable mercury isotopes. *Mar. Chem.* **2006,** *102*, (1-2), 134-147.
401 8. Hintelmann, H.; Evans, R. D.; Villeneuve, J. Y., Measurement of mercury methylation in
402 sediments by using enriched stable mercury isotopes combined with methylmercury determination by
403 gas-chromatography inductively-coupled plasma-mass spectrometry. *J. Anal. At. Spectrom.* **1995,** *10*, (9),
404 619-624.
405 9. Hintelmann, H.; Keppel-Jones, K.; Evans, R. D., Constants of mercury methylation and
406 demethylation rates in sediments and comparison of tracer and ambient mercury availability. *Environ.*
407 *Toxicol. Chem.* **2000,** *19*, (9), 2204-2211.
408 10. Johnson, W. P.; Swanson, N.; Black, B.; Rudd, A.; Carling, G.; Fernandez, D. P.; Luft, J.; Van
409 Leeuwen, J.; Marvin-DiPasquale, M., Total- and methyl-mercury concentrations and methylation rates
410 across the freshwater to hypersaline continuum of the Great Salt Lake, Utah, USA. *Sci. Total Environ.*
411 **2015,** *511*, 489-500.
412 11. Jonsson, S.; Skyllberg, U.; Nilsson, M. B.; Westlund, P. O.; Shchukarev, A.; Lundberg, E.; Bjorn,
413 E., Mercury methylation rates for geochemically relevant Hg-II species in sediments. *Environ. Sci.*
414 *Technol.* **2012,** *46*, (21), 11653-11659.
415 12. Korthals, E. T.; Winfrey, M. R., Seasonal and spatial variations in mercury methylation and
416 demethylation in an oligotrophic lake. *Appl. Environ. Microbiol.* **1987,** *53*, (10), 2397-2404.
417 13. Lehnherr, I.; St Louis, V. L.; Hintelmann, H.; Kirk, J. L., Methylation of inorganic mercury in
418 polar marine waters. *Nat. Geosci.* **2011,** *4*, (5), 298-302.
419 14. Martin-Doimeadios, R. C.; Tessier, E.; Amouroux, D.; Guyoneaud, R.; Duran, R.; Caumette, P.;
420 Donard, O. F. X., Mercury methylation/demethylation and volatilization pathways in estuarine sediment
421 slurries using species-specific enriched stable isotopes. *Mar. Chem.* **2004,** *90*, (1-4), 107-123.
422 15. Marvin-DiPasquale, M.; Windham-Myers, L.; Agee, J. L.; Kakouros, E.; Kieu, L. H.; Fleck, J.
423 A.; Alpers, C. N.; Stricker, C. A., Methylmercury production in sediment from agricultural and non-
424 agricultural wetlands in the Yolo Bypass, California, USA. *Sci. Total Environ.* **2014,** *484*, 288-299.
425 16. Marvin-DiPasquale, M. C.; Lutz, M. A.; Krabbenhoft, D. P.; Aiken, G. R.; Orem, W. H.; Hall, B.
426 D.; DeWild, J. F.; Brigham, M. E. *Total mercury, methylmercury, methylmercury production potential,*
427 *and ancillary streambed-sediment and pore-water data for selected streams in Oregon, Wisconsin, and*
428 *Florida, 2003–04*; U.S. Geological Survey Data Series 375: 2008; p 24 p.
429 17. Monperrus, M.; Tessier, E.; Amouroux, D.; Leynaert, A.; Huonnic, P.; Donard, O. F. X., Mercury
430 methylation, demethylation and reduction rates in coastal and marine surface waters of the Mediterranean
431 Sea. *Mar. Chem.* **2007,** *107*, (1), 49-63.
432 18. Olsen, T. A.; Brandt, C. C.; Brooks, S. C., Periphyton biofilms influence net methylmercury
433 production in an industrially contaminated system. *Environ. Sci. Technol.* **2016,** *50*, (20), 10843-10850.

19. Zhang, T.; Kucharzyk, K. H.; Kim, B.; Deshusses, M. A.; Hsu-Kim, H., Net methylation of mercury in estuarine sediment microcosms amended with dissolved, nanoparticulate, and microparticulate mercuric sulfides. *Environ. Sci. Technol.* **2014,** *48*, (16), 9133-9141.
20. Ramlal, P. S.; Rudd, J. W. M.; Hecky, R. E., Methods for measuring specific rates of mercury methylation and degradation and their use in determining factors controlling net rates of mercury methylation. *Appl. Environ. Microbiol.* **1986,** *51*, (1), 110-114.
21. Schaefer, J. K.; Morel, F. M. M., High methylation rates of mercury bound to cysteine by *Geobacter sulfurreducens*. *Nat. Geosci.* **2009,** *2*, (2), 123-126.
22. Schaefer, J. K.; Rocks, S. S.; Zheng, W.; Liang, L. Y.; Gu, B. H.; Morel, F. M. M., Active transport, substrate specificity, and methylation of Hg(II) in anaerobic bacteria. *Proceedings of the National Academy of Sciences of the United States of America* **2011,** *108*, (21), 8714-8719.
23. King, J. K.; Saunders, F. M.; Lee, R. F.; Jahnke, R. A., Coupling mercury methylation rates to sulfate reduction rates in marine sediments. *Environ. Toxicol. Chem.* **1999,** *18*, (7), 1362-1369.
24. Pham, A. L. T.; Johnson, C.; Manley, D.; Hsu-Kim, H., Influence of sulfide nanoparticles on dissolved mercury and zinc quantification by diffusive gradient in thin-film passive samplers. *Environ. Sci. Technol.* **2015,** *49*, (21), 12897-12903.
25. Bloom, N. S.; Preus, E.; Katon, J.; Hiltner, M., Selective extractions to assess the biogeochemically relevant fractionation of inorganic mercury in sediments and soils. *Anal. Chim. Acta* **2003,** *479*, (2), 233-248.
26. Liang, L.; Horvat, M.; Alvarez, J.; Young, L.; Kotnik, J.; Zhang, L., The challenge and its solution when determining biogeochemically reactive inorganic mercury (RHg): Getting the analytical method right. *American Journal of Analytical Chemistry* **2013,** *4*, (11), 10.
27. Hsu-Kim, H.; Kucharzyk, K. H.; Zhang, T.; Deshusses, M. A., Mechanisms regulating mercury bioavailability for methylating microorganisms in the aquatic environment: A critical review. *Environ. Sci. Technol.* **2013,** *47*, (6), 2441-2456.
28. Cannavo, F., Sensitivity analysis for volcanic source modeling quality assessment and model selection. *Computers & Geosciences* **2012,** *44*, 52-59.
29. U.S. Environmental Protection Agency *Method 1631, revision E: Mercury in water by oxidation, purge and trap, and cold vapor atomic fluorescence spectrometry*; EPA-821-R-02-019; Washington, D.C., 2002.
30. U.S. Environmental Protection Agency *Method 1630: Methyl mercury in water by distillation, aqueous ethylation, purge and trap, and cold vapor atomic fluorescence spectrometry*; EPA-821-R-01-020; Washington, D.C., August, 1998.
31. Amacher, M. C.; Selim, H. M.; Iskandar, I. K., Kinetics of mercuric-chloride retention by soils. *J. Environ. Qual.* **1990,** *19*, (3), 382-388.
32. Kim, Y. J.; Brooks, S. C.; Zhang, F.; Parker, J. C.; Moon, J. W.; Roh, Y., Fate and transport of uranium (VI) in weathered saprolite. *J. Environ. Radioact.* **2015,** *139*, 154-162.
33. Largitte, L.; Pasquier, R., A review of the kinetics adsorption models and their application to the adsorption of lead by an activated carbon. *Chem. Eng. Res. Des.* **2016,** *109*, 495-504.
34. Painter, S.; Cvetkovic, V.; Pickett, D.; Turner, D. R., Significance of kinetics for sorption on inorganic colloids: Modeling and experiment interpretation issues. *Environ. Sci. Technol.* **2002,** *36*, (24), 5369-5375.
35. Paria, S.; Manohar, C.; Khilar, K. C., Kinetics of adsorption of anionic, cationic, and nonionic surfactants. *Ind. Eng. Chem. Res.* **2005,** *44*, (9), 3091-3098.
36. Jonsson, S.; Skyllberg, U.; Nilsson, M. B.; Lundberg, E.; Andersson, A.; Bjorn, E., Differentiated availability of geochemical mercury pools controls methylmercury levels in estuarine sediment and biota. *Nat. Commun.* **2014,** *5*, 10.
37. Zhu, W.; Song, Y.; Adediran, G. A.; Jiang, T.; Reis, A. T.; Pereira, E.; Skyllberg, U.; Björn, E., Mercury transformations in resuspended contaminated sediment controlled by redox conditions, chemical speciation and sources of organic matter. *Geochim. Cosmochim. Acta* **2018,** *220*, 158-179.

38. Dagan, G.; Cvetkovic, V.; Shapiro, A., A solute flux approach to transport in heterogeneous formations: 1. The general framework. *Water Resources Research* **1992,** *28*, (5), 1369-1376.

FIGURE CAPTIONS

Figure 1. Hg methylation/MMHg demethylation conceptual model incorporating changing Hg/ MMHg availability. Subscripted "f" refers to fast sorption sites and the subscripted "s" refers to slow sorption sites. See Methods for explanation of symbols.

Figure 2. Changing Hg availability over time. Fraction of total Hg as dissolved Hg (red circles), sorbed Hg (blue squares), and Hg^0 (green diamonds) versus time. Solid lines correspond to the model fit to the data and 95% confidence bands were determined from Monte Carlo analysis (N = 10,000).

Figure 3. Changing MMHg availability over time. Fraction of total added MMHg remaining in dissolved phase (red circles) versus time. Red line corresponds to the model fit to the data; blue line represents the simulated sorbed MMHg. The 95% confidence bands were determined from Monte Carlo analysis (N = 10,000).

Figure 4. Model fit to the methylation/demethylation data sets. (a) ^{201}Hg methylation data set and (b) $MM^{202}Hg$ data set[18]. The red and blue lines are the model fit to the Hg methylation and MMHg demethylation data, respectively. The 95% confidence bands around the lines were determined from Monte Carlo analysis (N = 10,000).

Figure 5. Forward model simulations to examine model behavior. (a) Methylation, and (b) Demethylation tracer.

Figure 6. MMHg molar fraction in steady state versus travel time through a hypothetical periphyton bed. The upper curve (black line) accounts for transient availability in analyzing the methylation experiments and in the field-scale transport model. The lower curve (red line) assumes full availability at all times.

511 Figure 1

512

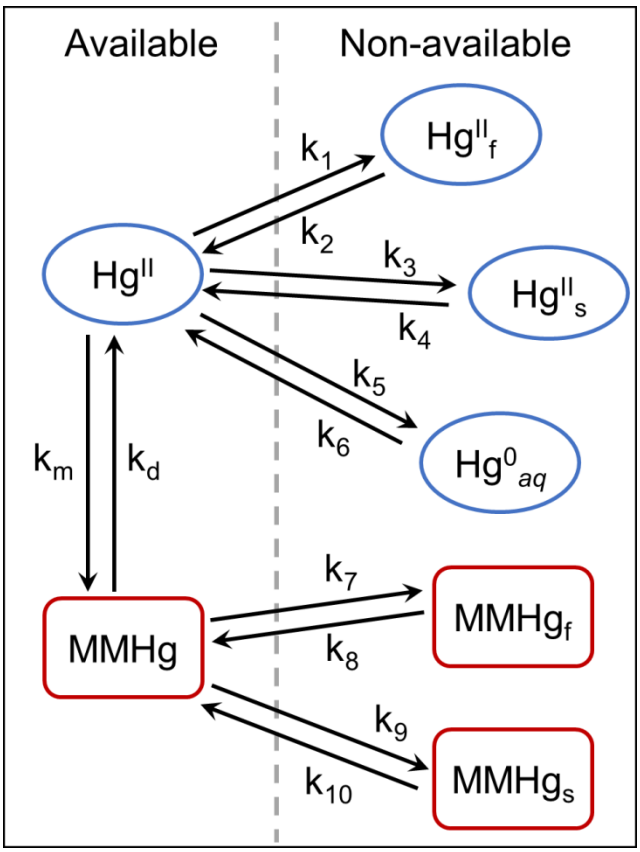

513

514

515

516 Figure 2

517

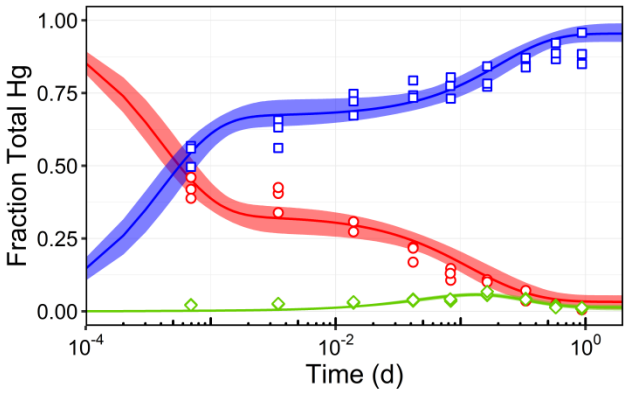

518

519 Figure 3

520

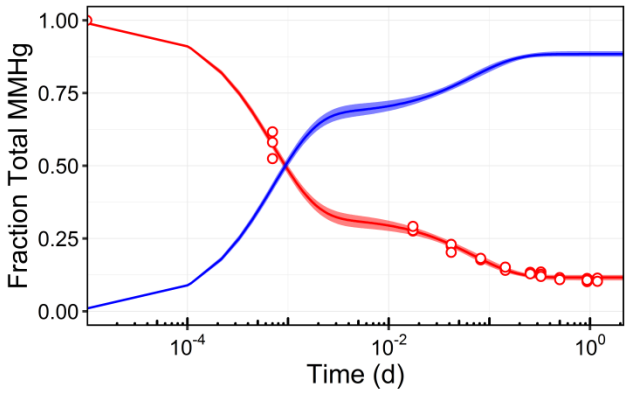

521

522

523 Figure 4

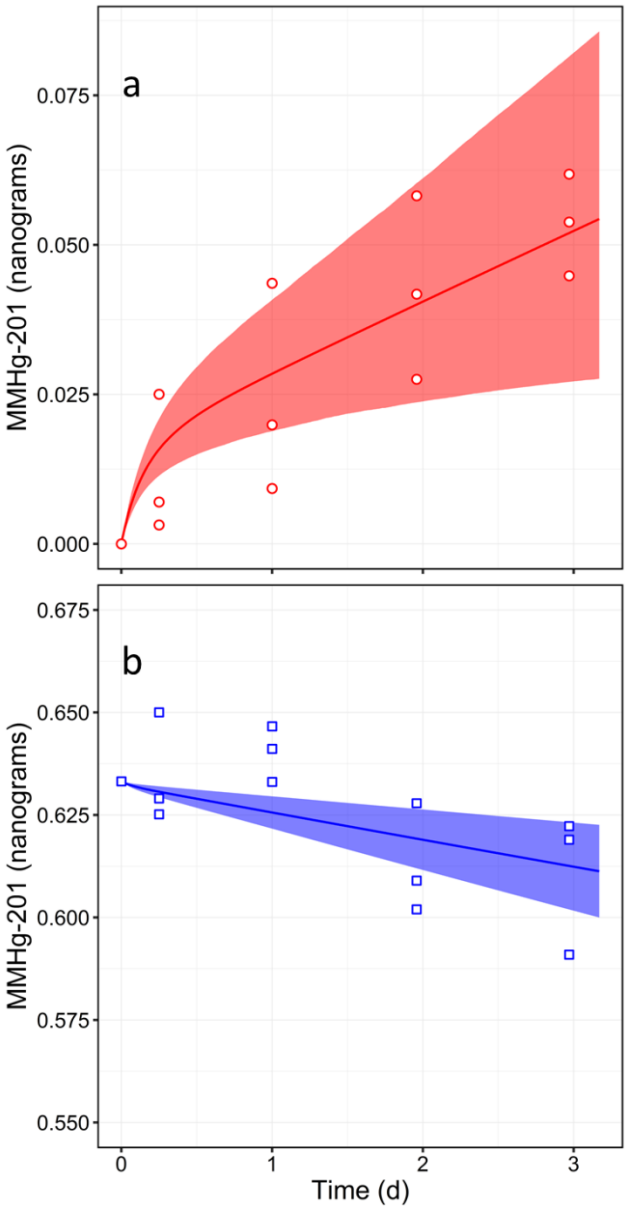

524

525

526 Figure 5

527

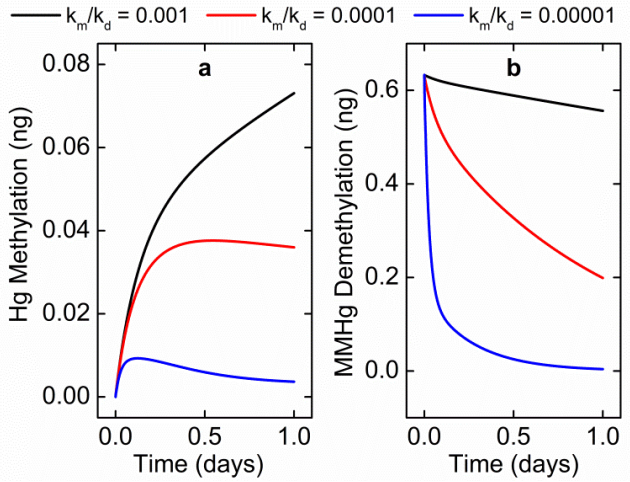

528

529

530 Figure 6

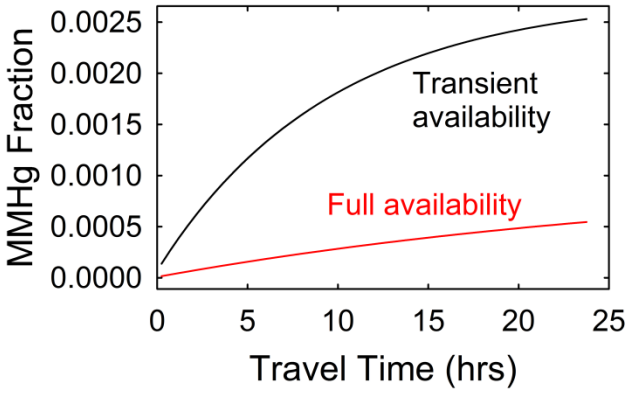

531

532

533